UC Irvine
UC Irvine Previously Published Works

Title

Correlation and Agreement of Yttrium-90 Positron Emission Tomography/Computed Tomography with Ex Vivo Radioembolization Microsphere Deposition in the Rabbit VX2 Liver Tumor Model

Permalink

https://escholarship.org/uc/item/7114s0sp

Journal

Journal of Vascular and Interventional Radiology, 32(1)

ISSN

1051-0443

Authors

Gordon, Andrew C
Gates, Vanessa L
White, Sarah B
et al.

Publication Date

2021

DOI

10.1016/j.jvir.2020.09.016

Peer reviewed

Correlation and Agreement of ^{90}Y PET/CT with Ex Vivo Radioembolization Microsphere Deposition in the Rabbit VX2 Liver Tumor Model

Andrew C. Gordon, MD, PhD[1,2], **Vanessa L. Gates, MS**[1], **Sarah B. White, MD, MS**[3], **Kathleen R. Harris, BA**[1], **Daniel Procissi, PhD**[1], **Zhuoli Zhang, MD, PhD**[1], **Weiguo Li, PhD**[1], **Donald Samaan, BA**[4], **Jodi R. Nicolai, MS**[1], **Samdeep K. Mouli, MD, MS**[1], **Kent T. Sato, MD**[1], **Robert K. Ryu, MD**[5], **Reed A. Omary, MD, MS**[6], **Riad Salem, MD, MBA**[1,7,8], **Robert J. Lewandowski, MD**[1,7,8], **Andrew C. Larson, PhD**[1,2]

[1.]Department of Radiology, Northwestern University, Feinberg School of Medicine, Chicago, IL, USA

[2.]Department of Biomedical Engineering, Northwestern University, Evanston, IL, USA

[3.]Department of Radiology, Division of Vascular & Interventional Radiology, Medical College of Wisconsin, Milwaukee, WI, USA

[4.]Medical Health Physics, Stanford University, Palo Alto, CA, USA

[5.]Department of Radiology, University of Colorado, Colorado, Aurora, CO, USA

[6.]Department of Radiology and Radiological Sciences, Vanderbilt University, Nashville, TN, USA

[7.]Department of Medicine, Hematology/Oncology, Northwestern University Feinberg School of Medicine, Chicago, IL, USA

[8.]Department of Surgery, Organ Transplantation, Northwestern University Feinberg School of Medicine, Chicago, IL, USA

Abstract

PURPOSE: To demonstrate stronger correlation and agreement of ^{90}Y PET/CT measurements with explant liver tumor dosing compared to the Standard Model (SM) for radioembolization.

MATERIALS and METHODS: Hepatic VX2 tumors were implanted into New Zealand White rabbits with growth confirmed on 7T MRI. Seventeen VX2 rabbits provided 33 analyzed tumors.

First/Corresponding Author: Andrew C. Gordon, MD-PhD, address below, andrew-gordon@northwestern.edu.
Senior Author: Andrew C. Larson, PhD, Professor, Department of Radiology, Northwestern University Feinberg School of Medicine, 737 N. Michigan Ave, 16th Floor, Chicago, IL 60611, Tel/fax: (312) 926-3499 / (312) 926-5991, a-larson@northwestern.edu

Treatment volumes were calculated with manually drawn volumes of interest (VOI) with 3D surface renderings. Radioembolization with glass ^{90}Y microspheres was performed. PET/CT imaging (Siemens Biograph 40) was completed with scatter and attenuation correction. 3D ellipsoid VOI were drawn to encompass tumors on fused images. Tumors and livers were then explanted for inductively coupled plasma optical emission spectroscopy (ICP-OES) analysis of microsphere content. ^{90}Y PET/CT and SM measurements were compared to reference standard ICP-OES measurements of tumor dosing with Pearson correlation and Bland-Altman analyses for agreement testing with and without adjustment for tumor necrosis.

RESULTS: The median infused activity was 33.3 MBq (range, 5.9–152.9). The correlation between ^{90}Y PET/CT measurements and tumor dose was r=0.903 (p<0.001). The correlation between SM estimates and tumor dose was r=0.607 (p<0.001). Bland-Altman analyses showed that the SM tended to underestimate tumor dosing by a mean of –8.5Gy (CI, –26.3–9.3) and the degree of underestimation increased to a mean of –18.3Gy (CI, –38.5–1.9) after adjustment for tumor necrosis. ^{90}Y PET/CT had better agreement with reference tumor dosing than the SM both with and without adjustment for necrosis.

CONCLUSION: ^{90}Y PET/CT estimates were strongly correlated and had better agreement with reference measurements of tumor dosing than SM dosing.

Summary Statement:

^{90}Y PET/CT measurements were more strongly correlated and had better agreement with microsphere deposition in tumor tissues than Standard Model dosimetry.

Keywords

INTRODUCTION

Conventional dosing for glass ^{90}Y microspheres with the Medical Internal Radiation Dose (MIRD) approach and assumed homogeneously distributed activity throughout the target liver parenchyma is referred to as the Standard Model (SM) yet preferential microsphere uptake due to tumor hypervascularity in hepatocellular carcinoma (HCC) is a tenet of intra-arterial therapy[1,2]. Tumors have variable vascularity and flow dynamics resulting in highly heterogeneous microsphere distributions[3,4]. Nuclear imaging of tumor targeting with ^{90}Y microspheres is possible through the detection of either bremsstrahlung radiation with SPECT/CT or a low abundance of positrons detected on PET/CT (^{90}Y PET/CT)[5]. While SPECT/CT may provide excellent visualization of intrahepatic ^{90}Y distributions, these approaches are generally not quantitative though this is an active area of research[6,7]. Quantitative ^{90}Y PET/CT imaging techniques for estimating ^{90}Y dose to targeted tumors may be accomplished on a voxel-wise basis for dosimetry calculations as previously demonstrated with resin microspheres, a process termed the Local Deposition Method (LDM)[8]. ^{90}Y PET/CT may allow more informative inter-institutional comparisons of outcomes and patient-specific prognostic metrics to optimize future radioembolization protocols. However, additional evidence on the relationships between imaging-based

estimations and infused activity delivered to targeted tumors is needed to inform clinical practice.

The SM for dosimetry has been useful to safely treat patients but does not specify the dose to individual tumors. The purpose of this study was to demonstrate stronger correlation and agreement of ^{90}Y PET/CT measurements with explant liver tumor dosing compared to the Standard Model (SM) for radioembolization.

MATERIALS and METHODS

Study Design

Institutional animal care and use committee approval was obtained. All procedures were performed under institutional and Animal Research: Reporting In Vivo Experiments (ARRIVE) guidelines. Female White New Zealand rabbits weighing 3–3.5 kg were used (Covance Laboratories, Greenfield, IN). Tumors were allowed to grow to 1–2cm after VX2 implantation and each animal was scanned with magnetic resonance imaging (MRI) to confirm tumor growth prior to treatment.

VX2 Animal Model and US-guided Tumor Implantation

Anesthesia was administered with a mixture of ketamine hydrochloride (20–40mg/kg) and xylazine (3–5mg/kg) with intramuscular injection. Rabbits received supplemental isoflurane (1.5–3%) via nosecone for maintenance during procedures. The implemented approach for ultrasound-guided tumor implantation has been previously described[9]. Rabbits were implanted with 2–3 tumors, preferentially in the left lobe; however, if space in the left lobe was limited, we would implant in the right lobe to mitigate tumors colliding/growing into one another. Additional implantation (up to 5 total) was performed if the tumor fragment was non-visualized within the liver by ultrasound immediately after implantation.

MR Imaging Protocols

Tumor growth was confirmed on MRI using a 20-cm bore Bruker ClinScan 7-Tesla magnet (Bruker Biospin MRI GmbH, Ettlingen, Germany). Respiratory gated, free-breathing acquisitions in both the coronal and axial planes were performed with T2-weighted (T2w) turbo spin echo (TSE) scans for a multi-slice acquisition providing complete coverage of the liver.

T2w TSE MRI parameters were TR/TE=1053/30ms; slice thickness=1.5mm; FOV=130×130mm^2; 1 average; 3 concatenations; FA=180°; 256×256 matrix (readoutsxphase-encodes); bandwidth=200Hz/Px; interleaved; respiratory gated (voxel size, 0.484×0.484×1.5mm^3). On T2w images, long- and short-axis tumor measurements in the axial plane were recorded. The treatment territory was determined based on catheter tip positioning at the time of radioembolization similar to the clinical paradigm. The target hepatic region was manually contoured on each slice based on the treatment territory. A three-dimensional surface rendering was performed in OsiriX software (v5.6, OsiriX Foundation, Geneva, Switzerland) for MRI volumetry to calculate the treatment volume in cc and then convert to mass (M) in kg by 1.03×10^{-3} kg/cc.

Standard Model Dosimetry

The estimated absorbed dose using the Standard Model was obtained assuming uniform distributions in tumor and normal hepatic tissue compartments as previously described[1,2].The dose to the treatment volume is given by:

$$D = \frac{50A(1 - LSF)(1 - R)}{M}$$

where D is the dose to the treated volume in Gy, A is the activity in GBq, M is the mass of treated tissue in kg, LSF (lung shunt fraction) refers to the fraction of microspheres delivered to the animal's lungs, and R is the fraction of residual activity in the dose vial. The fraction of microspheres deposited in the lungs was assumed to be negligible in comparison to hepatic microsphere uptake for treatment planning purposes based on past literature reporting no observed pulmonary deposition after intra-arterial infusion of smaller microspheres in this model[10].

^{90}Y Radioembolization

Radioembolization was performed by infusing 20–30 μm glass ^{90}Y microspheres (TheraSphere®, BTG) followed by 30–40cc of sterile 0.9% saline over 3–5 minutes, depending on native vessel flow rates. Dose vials calibrated at 1-, 3-, or 5-GBq were infused into each animal, and treatments occurred within 24hrs of baseline MRI. Following infusion, the catheter and sheath were removed, and hemostasis was achieved via ligation of the femoral artery. Euthasol (150–200mg/kg) was the euthanizing agent and introduced via the ear vein.

^{90}Y PET/CT Dosimetry

Following euthanasia of each rabbit, imaging was performed on a clinical PET/CT system (Biograph 40) with Pico-3D, Hi-REZ, and TrueV PET options and Sensation S-B40 CT option (Siemens Medical Solutions USA, Inc.). The specifications and sensitivity of this PET/CT system for clinical imaging of ^{90}Y have been previously reported[11]. PET acquisition was performed after initial localizing scan to define the field-of-view (FOV), including the liver and lungs. Total PET acquisition time was 60 minutes. Images were acquired in list-mode, and the resulting net trues sinogram was used for the reconstruction. Reconstructions were performed with corrections for randoms and scatter using iterative reconstruction with segmented attenuation correction with the following parameters: True-X, a proprietary PSF reconstruction; 3 iterations; 21 subsets; 4mm post-processing filter; 4mm loop filter; and a 4mm Gaussian smooth filter (4.07×4.07×5.00mm^3 voxel; 74 slices, 168×168 matrix). 3D ellipsoid volumes of interests (VOI) were drawn in Syngo TrueD to encompass tumors on fused PET/CT images while viewing side-by-side T2w MRI for anatomical correlation and thresholding to contour each tumor visually. The tumor dose on PET/CT was calculated on a voxel-wise basis by LDM:

PET/CT Dose (Gy) = 50 [Calibration Factor GBq ^{90}Y / Bq ^{86}Y] * [mean PET Activity Bq ^{86}Y] / [Tumor volume cc * 1.03×10^{-3}kg/cc]

Infused activity was equal to (1-R)*A. This was calculated based on the dose vial activity (A) at the time of infusion and the fraction of residual activity (R) not infused. The implemented calibration factor was generated from a linear fit of dose vial scans over known activities (R^2=0.999) specific to the scanner and scanning protocol described above[12].

Dose-Volume Histograms

VOI on activity maps were drawn using the fused anatomical CT images to encompass whole tumors and normal liver using VivoQuant software 2.0 (inviCRO LLC, Boston, MA, USA). Mean activity measurements were used to calculate absorbed dose in Gy on a voxel-by-voxel basis and converted into dose-volume histograms (DVHs) for tumor and normal liver VOI.

ICP-OES and Ex Vivo Microsphere Quantification

After completion of PET/CT imaging, all animals were frozen at −20°C for 30d to allow for 10 half-lives of ^{90}Y decay. After this decay period, rabbits were thawed slowly to room temperature over 48hrs, and necropsy was performed.

Tumors were given a unique ID for correlation to PET/CT images. Sections of tumor and normal hepatic parenchyma (NHP) from the right and left lobe weighing approximately 100–800mg were used for inductively coupled plasma optical emission spectroscopy (ICP-OES), a technique for quantitative measurements of metallic elemental concentrations. For each animal, samples consisted of sectioned tumor specimens for inclusion of the whole tumor; cubes of NHP taken from the right median lobe, left lateral lobe, and ± caudate lobe (2 each). These tissue samples were immediately weighed and stored at −20°C in metal-free 1 ml tubes until elemental microanalysis was performed by technical experts blinded to the PET/CT imaging results at an outside institution. All samples were digested in a 6mL cocktail of pure grade HNO_3 and a single drop of hydrofluoric acid. Microwave digestion was performed at 200°C in a PerkinElmer (Anton Paar) Multiwave 3000 microwave digester outfitted with a high-pressure rotor for digestion at 70 bar. Samples were analyzed on a PerkinElmer Optima 2000DV ICP-OES spectrometer in radial mode. Three to five runs per sample were averaged with quality control measurements confirming 92–98% accuracy. Matrix matching was used with a blank and two standards.

Tissue microsphere content was quantified for ceramic glass ^{90}Y microspheres ($17pY_2O_3.19qSiO_2.64rAl_2O_3$)[13]. Quantification for aluminum (Al) was chosen over silicon (Si) due to complex silicon chemistry, over zirconium (^{90}Zr), the decay product of ^{90}Y, due to the inability to distinguish this isotope from background hepatic Zr content, and given the relative scarcity of Al within hepatic tissues (reported to be 116±74 micrograms / kg wet tissue)[14,15]. This allowed calculation of microsphere ppm (mg microspheres / kg tissue) based on tissue Al ppm contents that exceeded these literature values by a factor of 10^3–10^4. The reference standard dose to a given tumor was calculated as a weighted average of measurements for each ith cube of tumor tissue by:

ICP Dose (Gy) = 50 [Specific Activity GBq/mg] * Σ_i[Microspheres mg/kg × Tissue weight kg]$_i$ / Σ_i[Tissue weight kg]$_i$

The specific activity was derived from the calibrated activity provided by the manufacturer and dose vial size (mg) and adjusted based on the time of infusion. Whole tumor samples may contain variable degrees of viable versus non-viable necrotic tissues. Therefore, reference standard dosing could in theory be influenced by necrotic volume percentage. To adjust for this potential confounder, necrotic volume was estimated based on T2w MRI images. The necrotic volume was divided by the whole tumor volume for estimation of the necrotic fraction. Viable ICP sample weight was calculated by viable weight = total weight * (1 – necrotic fraction).

Statistical Analyses

All data were analyzed with the statistical package STATA (version 14, StataCorp, College Station, Texas). ^{90}Y PET/CT measurements were performed prior to liver explant and tumors that did not appear in baseline imaging but identified on pathology were not retrospectively included. Data are reported as medians with 95% confidence intervals (CI). The Pearson correlation coefficient was used to evaluate the correlation between tumor dose on ICP and ^{90}Y PET/CT or SM dose estimates[16]. Concordance coefficients were also calculated in each case with 95% confidence intervals to determine whether the relationships between these measurements were reproducible. With an estimate of r=0.5, 29 tumors provided 80% power at alpha=0.05. A clustering analysis was performed for tumor measurements to examine the impact of clustering by rabbit on standard errors and interpretation of ordinary least squares (OLS) regression for each comparison. Bland-Altman analyses were also completed to test agreement between ^{90}Y PET/CT and SM dose estimates and tumor dose on ICP as the reference standard with and without correction for tumor necrosis as described above[17]. All analyses were two-tailed and considered statistically significant at *P* values less than 0.05.

RESULTS

MR Imaging of VX2 Tumors

Tumors were confirmed on MRI in 18 implanted rabbits. Two rabbits (11.1%, 2/18) had left hepatic artery catheterization. Infusions in the proper hepatic artery resulted in whole liver treatment in the remaining 88.9% (16/18). In one case, necropsy revealed extrahepatic tumor growth between two adjacent liver lobes after treatment, and this rabbit/tumor was considered untreated and therefore excluded. The remaining 17 rabbits provided 34 total intrahepatic VX2 tumors (mean 1.9±0.7 tumors / rabbit). The mean long-axis of these tumors measured 1.4cm (CI: 1.2–1.7) on anatomic T2-weighted MRI in the axial plane. Tumors were 22.8% (CI: 18.2–27.4) necrotic on average.

^{90}Y Radioembolization

Radioembolization was performed in all 18 rabbits. The median time to radioembolization after tumor implantation was 23.5d (CI: 20.0–29.3). Median administered activity after accounting for residual was 33.3MBq (CI: 27.0–66.6). The median residual activity left in the delivery device was 35.3% (CI: 21.1–49.0).

^{90}Y PET/CT

Intrahepatic delivery of ^{90}Y microspheres was confirmed in 88.9% (16/18) of cases. Reasons for extrahepatic activity (n=2) identified on PET/CT were non-target delivery to the gastrointestinal tract and damage to the hepatic artery resulting in extravasation. Activity maps revealed highly heterogeneous microsphere distributions within hepatic tissues (Figure 1, 2).

Tissue Microsphere Content by ICP-OES

Of the 127 tumor specimens, one sample (Supplemental Figure 1) was considered a strong outlier because it was over 21 times the interquartile range (IQR; 374mg/kg) above the 75th percentile (416 mg/kg). Given the quality control accuracy of 98.3% and uniformity of the five runs, metal contamination of this sample was considered likely (possibly due to a metallic shaving from surgical instruments used for sample handling, dust, or other lab materials), and the tumor was excluded from the remaining analyses. The mean microsphere content in tumor tissue was 319.9mg/kg (CI: 189.4–450.5) vs 231.4mg/kg (CI: 148.5–314.3) in the liver. The concentration in viable tumor was 414.9mg/kg (CI: 252.9–576.9). Preferential tumor uptake was highly variable with T:N ratios of 0.1–8.1 before adjusting for necrotic fraction (Figure 3) and 0.1–9.4 after adjustment.

Dosimetry and Dose-Volume Histograms

The relationship between PET/CT measurements and explant tumor dosing are shown in Figure 4. The median target treatment volume was 71.0cc (CI: 60.2–79.0). SM doses according to pre-treatment 3D volumes generated on MRI ranged from 4.9–151.7 Gy. The maximum difference in dose for tumors within a shared treatment volume (n=14 rabbits with multifocal disease) was 20.7±23.7Gy on PET/CT versus 28.6±47.7Gy on ICP-OES (p=0.3331).

Correlations between ^{90}Y PET/CT measurements and whole tumor dose or viable tumor dose *ex vivo* were strongly positive with r=0.903 (p<0.001; concordance 0.814, CI: 0.734–0.895, p<0.001) and r=0.896 (p<0.001; concordance 0.776, CI: 0.689–0.864, p<0.001), respectively. SM dosing was moderately correlated with eventual tumor dose at r=0.607 (p<0.001; concordance 0.566, CI: 0.348–0.783, p<0.001) and r=0.553 (p=0.001; concordance 0.481, CI: 0.251–0.711, p<0.001) before and after adjusting for necrotic fraction, respectively. Clustering analyses for all OLS regressions resulted in a minimal relative increase in the standard errors of 1.57% and did not change the interpretation.

On Bland-Altman analyses (Figure 5), the SM tended to underestimate tumor dose, reflected by a mean of −8.5Gy (CI: −26.3–9.3) and the degree of underestimation increased to a mean of −18.3Gy (CI: −38.5–1.9) after adjustment for tumor necrosis. In comparison, ^{90}Y PET/CT measurements tended to overestimate tumor dose, reflected by a mean of 3.9Gy (CI: −7.3–15.2) and underestimated dose with a mean −5.8Gy (CI: −18.9–7.2) after adjustment for tumor necrosis. These estimates and confidence intervals demonstrate ^{90}Y PET/CT had better agreement than SM dosing both with and without adjustment for tumor necrosis.

Dose-volume histograms (DVH) were generated for rabbits demonstrating at least one tumor with either focal or peripheral tumor uptake (11/17 rabbits with 21 tumors). DVHs for each tumor and whole liver are shown in Figure 6. DVHs for tumors compared to normal liver had higher median doses and there was substantial variability among these tumors.

DISCUSSION

The Medical Internal Radiation Dose (MIRD) approach is routinely used in clinical practice to calculate dosing for dispensed radiopharmaceuticals in broad settings[18]. The application of MIRD in the SM for radioembolization dosimetry based on the intended treatment volume is a safe and reliable method for prescribing ^{90}Y activity in glass microspheres validated by several phase 1 and 2 trials[1,19,20]. With the advent of microcatheter technologies, it is now possible to target smaller portions of liver with escalated dosing strategies such as dosing with ablative intent in some cases but SM dosimetry provides no tumor-specific dosing information[21,22]. Increased dosing approaches are rapidly emerging in the clinical setting for treating HCC portal vein tumor thrombus[23] and to accomplish radiation segmentectomy[21,22] or lobectomy[24,25]. Patient-specific imaging strategies to assess and quantify tumor microsphere uptake are absolutely necessary, especially in the setting of multifocal disease and neoplasms with mixed hypovascular versus hypervascular tumors as microsphere distributions can be highly heterogeneous[26].

Microspheres concentrations corresponded to 18.2 ± 27.5 spheres/mm^3 (max, 161.4 spheres/mm^3) within tumors and 13.2 ± 19.7 spheres/mm^3 (max, 122.7 spheres/mm^3) within the NHP. Resin microsphere concentrations in human livers have previously been estimated at 3.5 spheres/mm^3 [27]. Increased NHP microsphere concentrations may be secondary to use of 9–54mg dose vials in smaller rabbit livers and clustering of microspheres may explain the T:N ratios observed. Increased microsphere clustering has been demonstrated after radioembolization in pigs with increasing microsphere number beyond 8-day post-calibration[28]. Adjusting for necrotic fraction did not improve the correlation with ^{90}Y PET/CT, but this may be a reflection of the VX2 model and treatment timing as the vast majority of tumors were relatively small (1–2cm) with 23% necrosis. Moreover, correlation between viable tumor dose and whole tumor doses for large (13cm) tumors with necrotic fractions of 10–19% was also observed by Lea et al. in the clinical setting[26].

The most important limitation is the lack of longitudinal outcomes data linking tumor dosing and response to treatment as tumor response is linked to improved survival and was a necessary condition for survival beyond 3 years in the absence of surgery[29,30]. Since survival studies in the VX2 rabbit model can be complicated by extrahepatic disease, the first step was to initially validate this quantitative imaging approach *ex vivo*. The heterogeneous distribution of these microspheres rendered an *in vitro* model inadequate though there is extensive phantom data for PET/CT and PET/MRI, primarily for resin microspheres[31,32]. The VX2 tumor blood supply is derived from the hepatic artery, similar to that of human HCC, and rabbit anatomy is sufficiently large to facilitate catheterization procedures that closely parallel the clinical paradigm in human transarterial therapies[33,34]. Though VX2 is a virus-induced anaplastic squamous cell carcinoma unlike HCC suggesting this model may not be an accurate surrogate for HCC tumor response, this animal model

allowed variable dosing and recovery of explanted tumors in an experimental setting. Beta radiation from ^{90}Y have high maximum penetration for brachytherapy (11mm max, 2.5mm average) and more sophisticated dosimetry models that include voxel-to-voxel interactions (cross-dose) are possible; however, given voxel sizes of 4.07mm, the benefits of the latter approaches remain unclear, particularly in the absence of commercially available ^{90}Y imaging protocols. Moreover, comparisons of the LDM versus dose-point kernel convolution support use of LDM, especially for VOI and comparable FWHM as those used herein[8]. Therefore, the objective of this study was to validate this more straightforward and perhaps more clinically applicable approach using a widely available scanner, scanning protocol, and software for clinical relevance.

^{90}Y PET/CT measurements were strongly correlated with tumor dose. This early work demonstrates the feasibility for ^{90}Y dosing with PET/CT estimations of delivery to liver tumors following radioembolization with glass microspheres. Future work correlating these quantitative assessments with other anatomical and functional imaging approaches for evaluation of tumor response may enable discovery of early nuclear imaging biomarkers.

Supplementary Material

Refer to Web version on PubMed Central for supplementary material.

Acknowledgements:

Abbreviations:

^{90}**Y PET/CT**	yttrium-90 positron emission tomography / computed tomography A, activity
CI	95% confidence interval
DVH	dose-volume histogram
FA	flip angle
FWHM	full-width-at-half-maximum
HCC	hepatocellular carcinoma

ICP-OES	inductively coupled plasma optical emission spectroscopy
LDM	local deposition method
MIRD	Medical Internal Radiation Dose
MRI	magnetic resonance imaging
NHP	normal hepatic parenchyma
OLS	ordinary least squares
R	residual activity
SM	Standard Model
SPECT	single photon emission computed tomography
T2w	T2-weighted
T:N	tumor:normal ratio
TSE	turbo spin echo
VOI	volumes of interests

REFERENCES

1. Salem R, Thurston KG. Radioembolization with 90Yttrium microspheres: a state-of-the-art brachytherapy treatment for primary and secondary liver malignancies. Part 1: Technical and methodologic considerations. J Vasc Interv Radiol. 2006;17(8):1251–1278. [PubMed: 16923973]

2. Salem R, Thurston KG. Radioembolization with 90yttrium microspheres: a state-of-the-art brachytherapy treatment for primary and secondary liver malignancies. Part 2: special topics. J Vasc Interv Radiol. 2006;17(9):1425–1439. [PubMed: 16990462]

3. Tsafnat N, Tsafnat G, Lambert TD, et al. Modelling heating of liver tumours with heterogeneous magnetic microsphere deposition. Phys Med Biol. 2005;50(12):2937–2953. [PubMed: 15930612]

4. Högberg J, Rizell M, Hultborn R, et al. Heterogeneity of microsphere distribution in resected liver and tumour tissue following selective intrahepatic radiotherapy. EJNMMI Res. 2014;4(1):48. [PubMed: 26116112]

5. Elschot M, Vermolen BJ, Lam MGEH, et al. Quantitative comparison of PET and Bremsstrahlung SPECT for imaging the in vivo yttrium-90 microsphere distribution after liver radioembolization. PLoS ONE. 2013;8(2):e55742. [PubMed: 23405207]

6. Ahmadzadehfar H, Duan H, Haug AR, et al. The role of SPECT/CT in radioembolization of liver tumours. Eur. J. Nucl. Med. Mol. Imaging. 2014;41 Suppl 1:S115–24. [PubMed: 24442600]

7. Garin E, Rolland Y, Laffont S, et al. Clinical impact of (99m)Tc-MAA SPECT/CT-based dosimetry in the radioembolization of liver malignancies with (90)Y-loaded microspheres. Eur. J. Nucl. Med. Mol. Imaging. 2016;43(3):559–575. [PubMed: 26338177]

8. Pasciak AS, Bourgeois AC, Bradley YC. A Comparison of Techniques for (90)Y PET/CT Image-Based Dosimetry Following Radioembolization with Resin Microspheres. Front Oncol. 2014;4:1–10. [PubMed: 24478982]

9. White SB, Chen J, Gordon AC, et al. Percutaneous Ultrasound Guided Implantation of VX2 for Creation of a Rabbit Hepatic Tumor Model. PLoS ONE. 2015;10(4):e0123888. [PubMed: 25853660]

10. Chen J, White SB, Harris KR, et al. Poly(lactide-co-glycolide) microspheres for MRI-monitored delivery of sorafenib in a rabbit VX2 model. Biomaterials. 2015;61:299–306. [PubMed: 26022791]

11. Gates VL, Esmail AAH, Marshall K, et al. Internal pair production of 90Y permits hepatic localization of microspheres using routine PET: proof of concept. J Nucl Med. 2011;52(1):72–76. [PubMed: 21149493]

12. King M, Gates V, Leonard S, et al. Determining a calibration factor for Y-90 activity using the Y-86 setting on PET/CT. Society of Nuclear Medicine Annual Meeting Abstracts. 2014;55(Supplement 1):2716.

13. Erbe EM, Day DE. Chemical durability of Y2O3•Al2O3•SiO2 glasses for the in vivo delivery of beta radiation. J. Biomed. Mater. Res. 1993;27(10):1301–1308. [PubMed: 8245044]

14. Val Du G, Grubb BR, Bentley PJ. Tissue distribution of subcutaneously administered aluminum chloride in weanling rabbits. J Toxicol Environ Health. 1986;19(1):97–104. [PubMed: 3746943]

15. Röllin HB, Theodorou P, Kilroe-Smith TA. Deposition of aluminium in tissues of rabbits exposed to inhalation of low concentrations of Al2O3 dust. Br J Ind Med. 1991;48(6):389–391. [PubMed: 2064977]

16. Zou KH, Tuncali K, Silverman SG. Correlation and simple linear regression. Radiology. 2003;227(3):617–622. [PubMed: 12773666]

17. Bland JM, Altman DG. Measuring agreement in method comparison studies. Stat Methods Med Res. 1999;8(2):135–160. [PubMed: 10501650]

18. Bolch WE, Bouchet LG, Robertson JS, et al. MIRD pamphlet No. 17: the dosimetry of nonuniform activity distributions--radionuclide S values at the voxel level. Medical Internal Radiation Dose Committee. J Nucl Med. 1999;40(1):11S–36S. [PubMed: 9935083]

19. Salem R, Lewandowski RJ, Atassi B, et al. Treatment of unresectable hepatocellular carcinoma with use of 90Y microspheres (TheraSphere): safety, tumor response, and survival. J Vasc Interv Radiol. 2005;16(12):1627–1639. [PubMed: 16371529]

20. Mazzaferro V, Sposito C, Bhoori S, et al. Yttrium-90 radioembolization for intermediate-advanced hepatocellular carcinoma: A phase 2 study. Hepatology. 2012;57(5):1826–1837.

21. Riaz A, Gates VL, Atassi B, et al. Radiation segmentectomy: a novel approach to increase safety and efficacy of radioembolization. Int J Radiat Oncol Biol Phys. 2011;79(1):163–171. [PubMed: 20421150]

22. Vouche M, Habib A, Ward TJ, et al. Unresectable solitary hepatocellular carcinoma not amenable to radiofrequency ablation: multicenter radiology-pathology correlation and survival of radiation segmentectomy. Hepatology. 2014;60(1):192–201. [PubMed: 24691943]

23. Garin E, Rolland Y, Edeline J, et al. Personalized dosimetry with intensification using 90Y-loaded glass microsphere radioembolization induces prolonged overall survival in hepatocellular carcinoma patients with portal vein thrombosis. J Nucl Med. 2015;56(3):339–346. [PubMed: 25678490]

24. Gaba RC, Lewandowski RJ, Kulik LM, et al. Radiation Lobectomy: Preliminary Findings of Hepatic Volumetric Response to Lobar Yttrium-90 Radioembolization - Springer. Ann Surg Oncol. 2009;16(6):1587–1596. [PubMed: 19357924]

25. Vouche M, Lewandowski RJ, Atassi R, et al. Radiation lobectomy: Time-dependent analysis of future liver remnant volume in unresectable liver cancer as a bridge to resection. J. Hepatol. 2013;59(5):1029–1036. [PubMed: 23811303]

26. Lea WB, Tapp KN, Tann M, et al. Microsphere Localization and Dose Quantification Using Positron Emission Tomography/CT following Hepatic Intraarterial Radioembolization with Yttrium-90 in Patients with Advanced Hepatocellular Carcinoma. JVIR. 2014;25(10):1595–1603. Available at: http://eutils.ncbi.nlm.nih.gov/entrez/eutils/elink.fcgi?dbfrom=pubmed&id=25156647&retmode=ref&cmd=prlinks. [PubMed: 25156647]

27. Campbell AM, Bailey IH, Burton MA. Analysis of the distribution of intra-arterial microspheres in human liver following hepatic yttrium-90 microsphere therapy. Phys Med Biol. 2000;45(4):1023–1033. [PubMed: 10795989]

28. Pasciak AS, Abiola G, Liddell RP, et al. The number of microspheres in Y90 radioembolization directly affects normal tissue radiation exposure. Eur. J. Nucl. Med. Mol. Imaging. 2020;47(4):816–827. [PubMed: 31741021]

29. Riaz A, Gabr A, Abouchaleh N, et al. Radioembolization for hepatocellular carcinoma: Statistical confirmation of improved survival in responders by landmark analyses. Hepatology. 2018;27:1485.

30. Gordon AC, Gabr A, Riaz A, et al. Radioembolization Super Survivors: Extended Survival in Non-operative Hepatocellular Carcinoma. Cardiovasc Inter Rad. 2018;41(10):1557–1565.

31. Willowson KP, Tapner M, QUEST Investigator Team, et al. A multicentre comparison of quantitative (90)Y PET/CT for dosimetric purposes after radioembolization with resin microspheres : The QUEST Phantom Study. Eur. J. Nucl. Med. Mol. Imaging. 2015;42(8):1202–1222. [PubMed: 25967868]

32. Maughan NM, Eldib M, Faul D, et al. Multi institutional quantitative phantom study of yttrium-90 PET in PET/MRI: the MR-QUEST study. EJNMMI Physics. 2018;5(1):7. [PubMed: 29616365]

33. Gupta T, Virmani S, Neidt TM, et al. MR tracking of iron-labeled glass radioembolization microspheres during transcatheter delivery to rabbit VX2 liver tumors: feasibility study. Radiology. 2008;249(3):845–854. [PubMed: 18840788]

34. Geschwind JF, Artemov D, Abraham S, et al. Chemoembolization of liver tumor in a rabbit model: assessment of tumor cell death with diffusion-weighted MR imaging and histologic analysis. J Vasc Interv Radiol. 2000;11(10):1245–1255. [PubMed: 11099235]
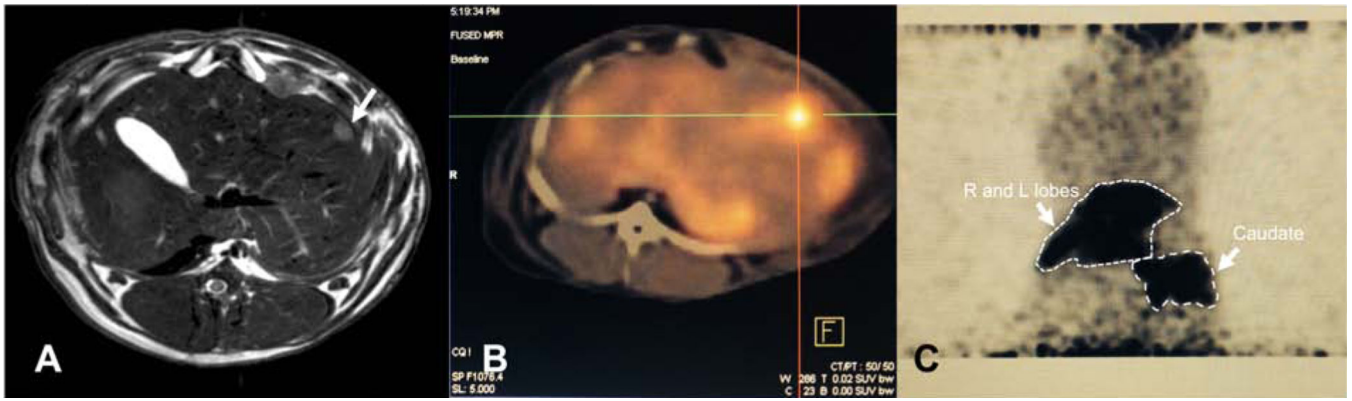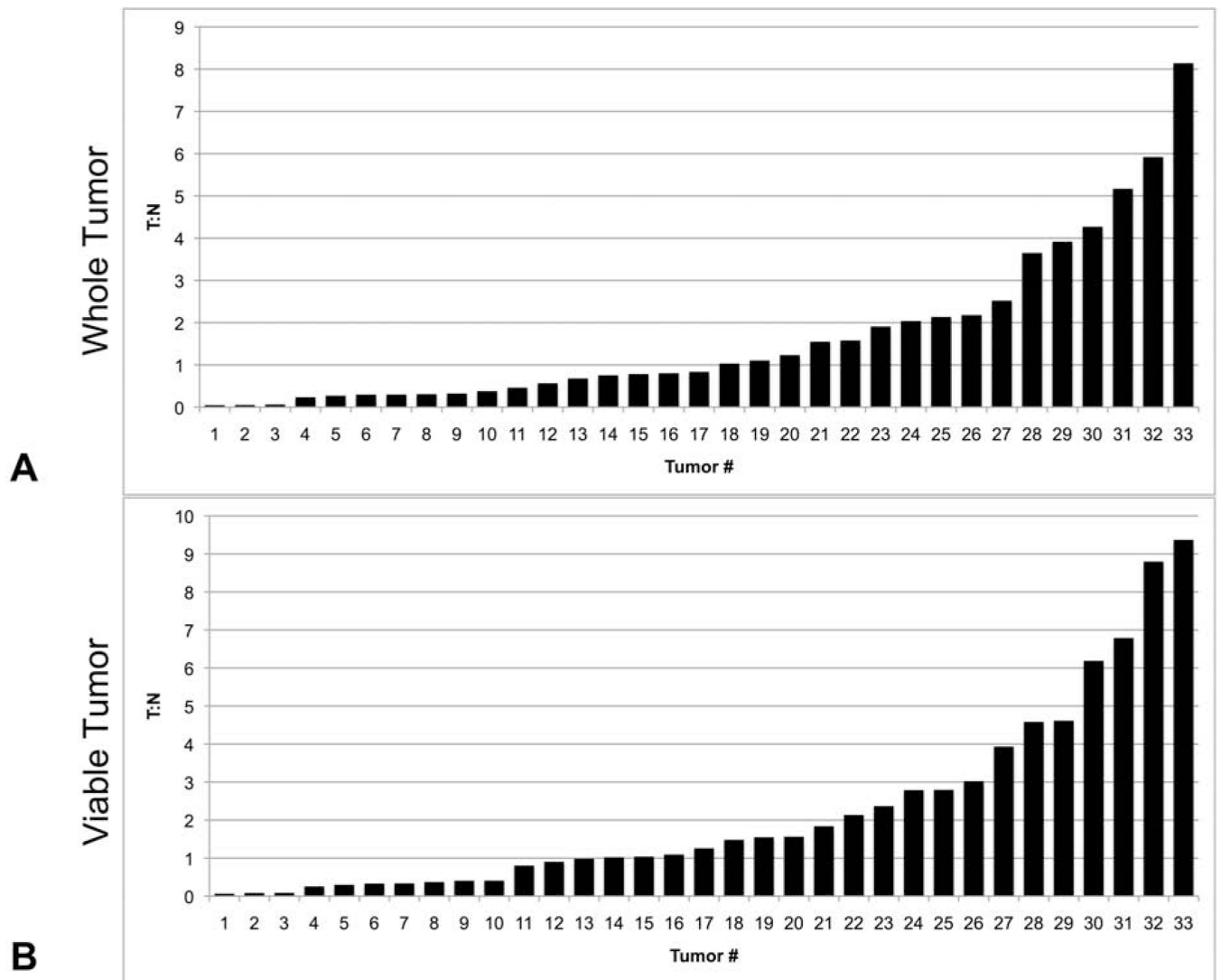
Figure 1.
Focal uptake of glass ^{90}Y microspheres was seen in 38.2% (13/34) of VX2 tumors on ^{90}Y PET/CT. (A) T2-w MRI demonstrates a small T2 hyperintense tumor (arrow) in the left lobe without central necrosis. (B) The fused ^{90}Y PET/CT image maps increased activity in the tumor with a heterogeneous distribution in the normal hepatic parenchyma. (C) Maximum intensity projection demonstrating the distribution of activity throughout the liver (including caudate lobe).
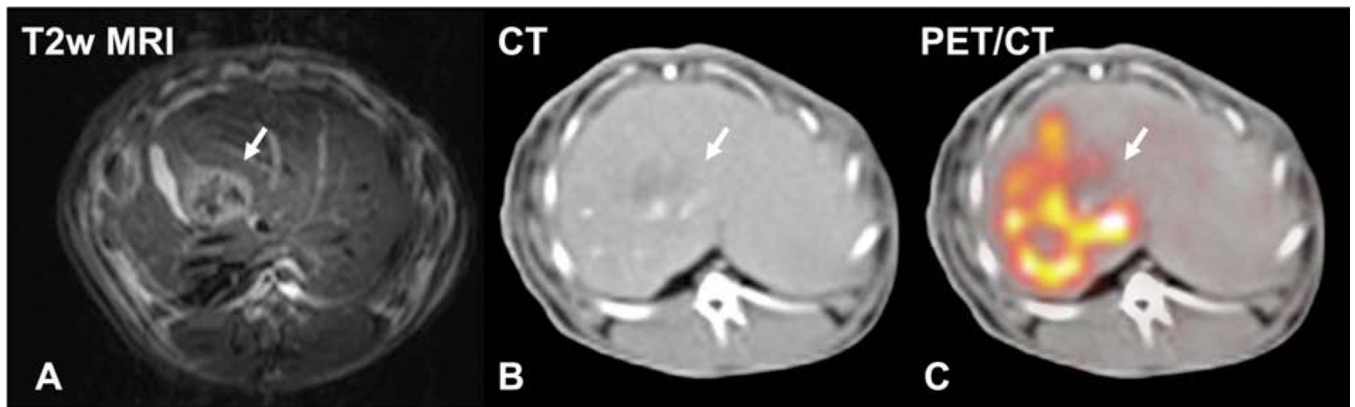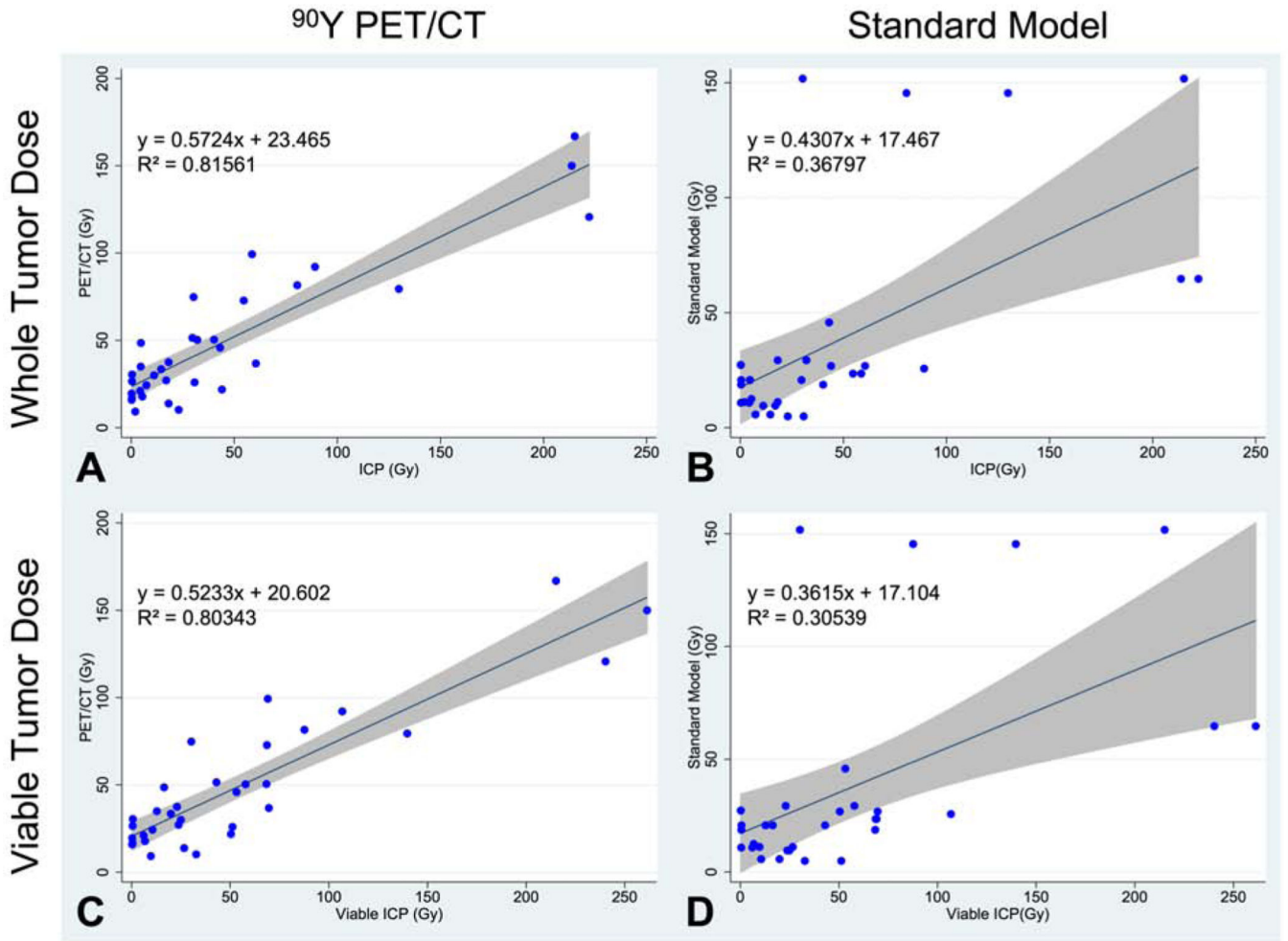
Figure 2.
Peripheral tumor uptake of ^{90}Y microspheres was observed in 17.7% (6/34) of VX2 tumors on ^{90}Y PET/CT. The VX2 rabbit was treated intra-arterially with 47.4 MBq glass ^{90}Y microspheres in the proper hepatic artery (PHA). (A) Axial MRI demonstrates a T2 hyperintense tumor (arrow) with central necrosis abutting the gallbladder. (B) The tumor is hypodense on non-contrast CT with areas of pooled contrast scattered throughout the right hepatic lobe. (C) The fused ^{90}Y PET/CT image maps activity preferentially to the tumor periphery and right hepatic lobe with relative sparring of the necrotic region, anteriomedial quadrant (arrow), and left hepatic lobe despite PHA infusion.
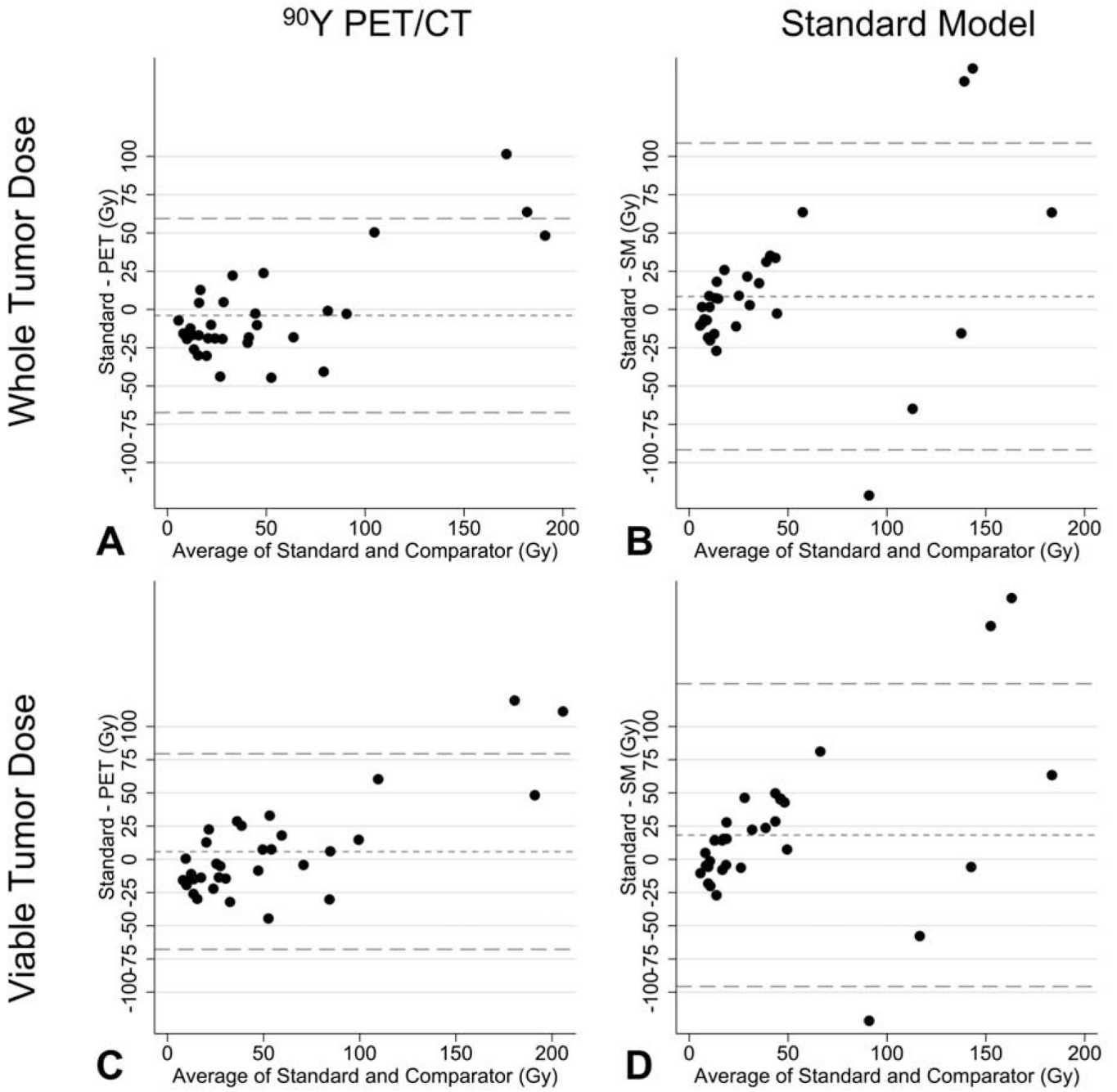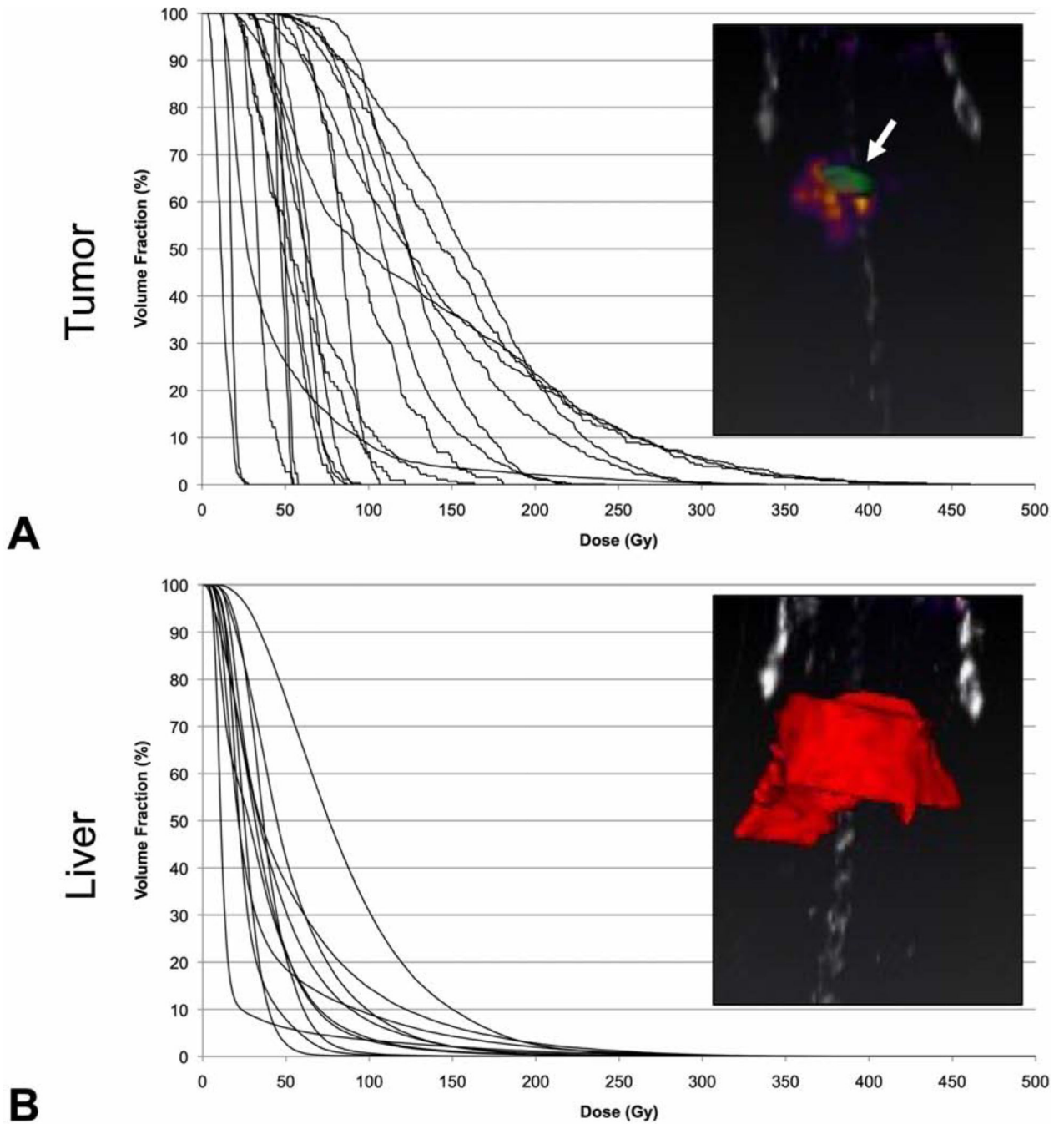
Figure 3.
Tumor:Normal ratios of microsphere concentration for each tumor without (top, A), and with (bottom, B) adjustment for tumor necrosis. Values >1.0 indicate preferential deposition of microspheres within tumor tissues. Tumor microsphere uptake relative to the normal liver was highly variable highlighting the importance of tumor-specific dosimetry.

Figure 4.
Scatter plots including linear regression and 95% confidence interval for tumor absorbed dose estimates after Standard Model (left) and ^{90}Y PET/CT (right) versus ICP on explant with (bottom) and without (top) correction for necrosis. (A) SM estimates assume equivalent dosing for tumors within a shared treatment volume and were moderately correlated with explanted doses. (B) Tumor ^{90}Y PET/CT dose estimates were strongly correlated with tumor ^{90}Y microsphere dose on explant. (C,D) Adjusting for the necrotic fraction yielded similar results in these small tumors. The y-intercepts indicated a noise floor of 20–23Gy for tumors imaged with ^{90}Y PET/CT (A,C).

Figure 5.

Bland-Altman plots show the difference against the mean value for (A) ^{90}Y PET/CT or (B) SM dose in Gy with ICP-OES tumor dosing as the reference standard. The *narrow dashed* lines represents the mean difference with 2 standard deviations denoted by the *wider dashed* lines. The mean difference for ^{90}Y PET/CT was closer to 0 and had decreased variance in comparison to the SM. (C,D) This was similarly true after adjusting for tumor necrosis.

Figure 6.
Dose-volume histograms for tumor (n=21) and liver tissues in rabbits (n=11) with focal or peripheral tumor uptake. Anatomical CT images were used to contour the liver (bottom) and individual tumors (top, arrow). Voxel-wise MIRD was applied to estimate dose within each voxel and quantification of the absorbed dose throughout the target volume. Tumor tissues (arrow) demonstrated varied dosing with a rightward shift in dose for a given volume compared to liver dosing.